

CHARACTERIZING TWO SOLAR-TYPE *KEPLER* SUBGIANTS WITH ASTEROSEISMOLOGY:
KIC 10920273 AND KIC 11395018

G. DOĞAN^{1,2,3}, T. S. METCALFE^{1,3,4}, S. DEHEUVELS^{3,5}, M. P. DI MAURO⁶, P. EGGENBERGER⁷, O. L. CREEVEY^{8,9,10}, M. J. P. F. G. MONTEIRO¹¹, M. PINSONNEAULT^{3,12}, A. FRASCA¹³, C. KAROFF², S. MATHUR¹, S. G. SOUSA¹¹, I. M. BRANDÃO¹¹, T. L. CAMPANTE^{11,18}, R. HANDBERG², A. O. THYGESEN^{2,14}, K. BIAZZO¹⁵, H. BRUNTT², E. NIEMCZURA¹⁶, T. R. BEDDING¹⁷, W. J. CHAPLIN^{3,18}, J. CHRISTENSEN-DALSGAARD^{2,3}, R. A. GARCÍA^{3,19}, J. MOLEND-ŽAKOWICZ¹⁶, D. STELLO¹⁷, J. L. VAN SADERS^{3,12}, H. KJELDSEN², M. STILL²⁰, S. E. THOMPSON²¹, AND J. VAN CLEVE²¹

¹ High Altitude Observatory, National Center for Atmospheric Research, P.O. Box 3000, Boulder, CO 80307, USA

² Stellar Astrophysics Centre, Department of Physics and Astronomy, Aarhus University, Ny Munkegade 120, DK-8000 Aarhus C, Denmark

³Kavli Institute for Theoretical Physics, Kohn Hall, University of California, Santa Barbara, CA 93106, USA

⁴ Space Science Institute, Boulder, CO 80301, USA

⁵Department of Astronomy, Yale University, PO Box 208101, New Haven, CT 06520-8101, USA

⁶ INAF-IAPS, Istituto di Astrofisica e Planetologia Spaziali, Via del Fosso del Cavaliere 100, 00133 Roma, Italy

⁷ Geneva Observatory, University of Geneva, Maillettes 51, 1290 Sauverny, Switzerland

⁸ Université de Nice, Laboratoire Cassiopée, CNRS UMR 6202, Observatoire de la Côte d'Azur, BP 4229, 06304 Nice cedex 4, France

⁹ IAC Instituto de Astrofísica de Canarias, C/ Vía Láctea s/n, E-38200 Tenerife, Spain

¹⁰ Universidad de La Laguna, Avda. Astrofísico Francisco Sánchez s/n, 38206 La Laguna, Tenerife, Spain

¹¹ Centro de Astrofísica and DFA-Faculdade de Ciências, Universidade do Porto, Portugal

¹²Ohio State University, Department of Astronomy, 140 W. 18th Ave., Columbus, OH 43210, USA

¹³ INAF, Osservatorio Astrofisico di Catania, via S. Sofia, 78, 95123, Catania, Italy

¹⁴ Zentrum für Astronomie der Universität Heidelberg, Landessternwarte, Königstuhl 12, 69117 Heidelberg, Germany

¹⁵ INAF - Osservatorio Astronomico di Capodimonte, Salita Moiariello 16, 80131, Napoli, Italy

¹⁶ Instytut Astronomiczny, Uniwersytet Wrocławski, ul. Kopernika 11, 51-622 Wrocław, Poland

¹⁷ Sydney Institute for Astronomy (SIfA), School of Physics, University of Sydney, NSW 2006, Australia

¹⁸ School of Physics and Astronomy, University of Birmingham, Edgbaston, Birmingham, B15 2TT, UK

¹⁹ Laboratoire AIM, CEA/DSM – CNRS – U. Paris Diderot – IRFU/Sap, Centre de Saclay, 91191 Gif-sur-Yvette Cedex, France

²⁰ Bay Area Environmental Research Institute / NASA Ames Research Center, Moffett Field, CA 94035, USA and

²¹ SETI Institute / NASA Ames Research Center, Moffett Field, CA 94035, USA

Draft version March 6, 2018

ABSTRACT

Determining fundamental properties of stars through stellar modeling has improved substantially due to recent advances in asteroseismology. Thanks to the unprecedented data quality obtained by space missions, particularly CoRoT and *Kepler*, invaluable information is extracted from the high-precision stellar oscillation frequencies, which provide very strong constraints on possible stellar models for a given set of classical observations. In this work, we have characterized two relatively faint stars, KIC 10920273 and KIC 11395018, using oscillation data from *Kepler* photometry and atmospheric constraints from ground-based spectroscopy. Both stars have very similar atmospheric properties; however, using the individual frequencies extracted from the *Kepler* data, we have determined quite distinct global properties, with increased precision compared to that of earlier results. We found that both stars have left the main sequence and characterized them as follows: KIC 10920273 is a one-solar-mass star ($M = 1.00 \pm 0.04M_{\odot}$), but much older than our Sun ($\tau = 7.12 \pm 0.47$ Gyr), while KIC 11395018 is significantly more massive than the Sun ($M = 1.27 \pm 0.04M_{\odot}$) with an age close to that of the Sun ($\tau = 4.57 \pm 0.23$ Gyr). We confirm that the high lithium abundance reported for these stars should not be considered to represent young ages, as we precisely determined them to be evolved subgiants. We discuss the use of surface lithium abundance, rotation and activity relations as potential age diagnostics.

Subject headings: asteroseismology — stars: evolution — stars: fundamental parameters — stars: individual (KIC 10920273, KIC 11395018) — stars: solar-type

1. INTRODUCTION

Classical modeling of single stars mostly relies on fitting to the atmospheric properties obtained through spectroscopic and/or photometric observations, such as effective temperature, surface gravity, and elemental abundances. This yields a large number of possible models covering a wide range of values for the fundamental properties, particularly in the absence of independent

radius and luminosity measurements. Asteroseismology has been revolutionizing stellar modeling as a result of the precise and accurate inferences on stellar structure that have been made possible by a new generation of asteroseismic observations. Stellar fundamental properties, particularly mass and radius, can be determined to a few percent uncertainty, even when only the average seismic parameters are used as additional constraints, with the precision on age determination being as good as $\sim 20\%$. The precision and accuracy of these properties increase

further when the individual oscillation frequencies are used (see, e.g., Mathur et al. 2012 for a comparison between using average and individual seismic quantities as constraints in the modeling of a large sample of *Kepler* stars). Moreover, the individual frequencies allow us to obtain information about the stellar interiors.

Asteroseismology has proved very effective in constraining the stellar age and the evolutionary stage with the help of specific features seen in the oscillation spectra. Mixed modes are particularly important in this regard. As a star evolves, the frequencies of the p modes decrease due to increasing stellar size, while the g-mode frequencies increase. By the time the star moves off the main sequence, the g- and p-mode trapping cavities are closer to each other, which results in the interaction of the two types of modes as they go through “avoided crossings”. The modes affected by this interaction are referred to as mixed modes due to having g-mode characteristics in the deep interior, and p-mode characteristics near the surface, of the star (see Osaki 1975 and Aizenman et al. 1977 for an introductory discussion). They are sensitive to the central conditions and hence encode information from the core, where the chemical composition changes due to the nuclear reactions driving the evolution of the star. Since the timescales of avoided crossings are very small compared to the stellar evolutionary timescale, mixed modes provide very strong constraints on the stellar age (see, e.g., Deheuvels & Michel 2011; Metcalfe et al. 2010; Benomar et al. 2012 for recent analyses).

Kepler is a space telescope with a diameter of 0.95 m that has been providing high-quality photometric data since the beginning of its operations in May 2009 (see, e.g., Borucki et al. 2010; Koch et al. 2010; Chaplin et al. 2010, 2011). The mission’s primary objective is to search for Earth-sized planets through the transit method. Asteroseismology is being used to characterize a subsample of stars, some of which host planets. *Kepler* monitors more than 150,000 stars, and ~ 2000 of these were selected to be monitored for one month each in short-cadence mode (58.9 s integrations) during the first ~ 10 months of the mission (Gilliland et al. 2010; Chaplin et al. 2011). Solar-like oscillations were detected in at least 500 of those survey stars (Chaplin et al. 2011). A subsample (~ 190) of these have been monitored for more than 3 months, and precise determination of the oscillation properties has been completed for part of the sample (Appourchaux et al. 2012). Asteroseismology has been proving successful in determining their global properties and inferring their interiors (see, e.g. Metcalfe et al. 2010, 2012; Creevey et al. 2012; Deheuvels et al. 2012; Mathur et al. 2012).

KIC 10920273 (kepmag=11.93 mag, i.e., apparent magnitude as observed through the *Kepler* bandpass) and KIC 11395018 (kepmag=10.76 mag) are among a handful of asteroseismic targets that were observed continuously from the start of science operations. Consequently, extended timeseries were available from early in the mission, making both stars attractive targets for asteroseismic analysis (Campante et al. 2011; Mathur et al. 2011). We also acquired ground-based spectra in order to characterize these stars. They are G-type stars with very similar spectroscopic properties, especially T_{eff} and $\log g$ (see, Sect. 2.1), so it is difficult to discriminate be-

tween models for the two stars using classical approaches. These approaches include matching the position of the star in the Hertzsprung-Russell (H-R) diagram in the form that shows luminosity versus effective temperature as the star evolves, or alternatively in the $\log g$ - T_{eff} diagram, given that the luminosity cannot be calculated using the available observations.

We present the observational data employed to characterize our stars in Section 2, our modeling approach in Section 3, and the results in Section 4, while Section 5 provides a summary and conclusions.

2. OBSERVATIONAL CONSTRAINTS

2.1. Atmospheric properties

Atmospheric properties of KIC 10920273 and KIC 11395018 were obtained from observations with the FIES spectrograph (Frandsen & Lindberg 1999) at the Nordic Optical Telescope (NOT on La Palma, Spain), at medium resolution ($R \sim 46,000$) in July and August 2010. The reduced spectra were analyzed by several teams and the results were presented by Creevey et al. (2012). The constraints we used for our analysis are shown in Table 1 (see also the 1- and 2- σ error boxes in Fig. 1). We adopted a set of atmospheric constraints for each star that were closest to the mean of results from several methods described by Creevey et al. (2012). This approach was preferred for the sake of reproducibility, rather than using the mean values. However, we did not restrict our model-searching space to less than 3- σ uncertainty around these constraints; therefore, the selected values represent well the overall results of the spectroscopic analysis.

The spectroscopic $v \sin i$ values for KIC 10920273 and KIC 11395018 are $1.5 \pm 2.2 \text{ km s}^{-1}$ and $1.1 \pm 0.8 \text{ km s}^{-1}$, respectively (Creevey et al. 2012). These low values indicate either slow rotation or low inclination angle i , although the latter is statistically unlikely. Rotational periods from modulation of the *Kepler* data due to spots on the surfaces of the two stars were measured to be ~ 27 days for KIC 10920273 (Campante et al. 2011), and ~ 36 days for KIC 11395018 (Mathur et al. 2011). The signal-to-noise ratios (SNR) of the peaks used for these measurements, particularly for KIC 10920273, were low, so the results should be used with caution. Mathur et al. (2011) inferred $i \geq 45^\circ$ for KIC 11395018 based on combining the rotational frequency splittings with the measured rotation period, which implies this star to be a slow rotator. A wider range of inclinations was possible for KIC 10920273 (Campante et al. 2011). However, the modulation in the light curve has been detected with less uncertainty in the new analysis performed using longer time series including *Kepler* Q9 and Q10 data of KIC 10920273 (García et al., private communication). If confirmed, this would be consistent with a relatively high inclination angle, and slow rotation. The effects of the centrifugal force are negligible for slowly rotating stars.¹ However, rotational mixing may lead to changes in the

¹ If, counter to our expectations, one of these stars were to be confirmed as a fast rotator, rotational effects on the oscillation frequencies would have to be taken into account (see Suárez et al. 2010 for a detailed analysis of the effects of centrifugal distortion on solar-like oscillations). Currently, there is no robust detection of rotational frequency splittings that can be included as constraints in our modeling.

TABLE 1
ADOPTED ATMOSPHERIC CONSTRAINTS FOR KIC 10920273
AND KIC 11395018 (FROM CREEVEY ET AL. 2012)

Star	T_{eff} (K)	$\log g$	[Fe/H]
KIC 10920273	5790 ± 74	4.10 ± 0.10	-0.04 ± 0.10
KIC 11395018	5700 ± 100	4.10 ± 0.20	0.13 ± 0.10

properties of the models even for slowly rotating stars, because the efficiency of this mixing is more directly related to differential rotation in stellar interiors rather than to surface rotational velocities (Pinsonneault et al. 1990; Eggenberger et al. 2010). Studying the impact of rotation on post-main-sequence stars would require a detailed discussion of the effects of rotational mixing on the chemical gradients in the central parts of the star. These influence the asteroseismic properties of the models, particularly the mixed modes. In the specific case of the evolved post-main-sequence stars modeled here, however, we expect that these effects on the chemical gradients would already be erased, as found by Miglio et al. (2007) for models of 12 Bootis A in the thick-shell-H-burning phase (see also the discussion of the effects of microscopic diffusion in the subgiant HD 49385 by Deheuvels & Michel 2011). We therefore have not included the rotational effects for most of the analyses (see Section 3).

When the atmospheric properties alone are considered, these two stars are very similar. Due to the degeneracy inherent in the H-R diagram analysis (see, e.g., Fernandes & Monteiro 2003), it is not possible to determine the global stellar properties with sufficiently high precision to study their detailed characteristics without the help of seismic data, which we now discuss.

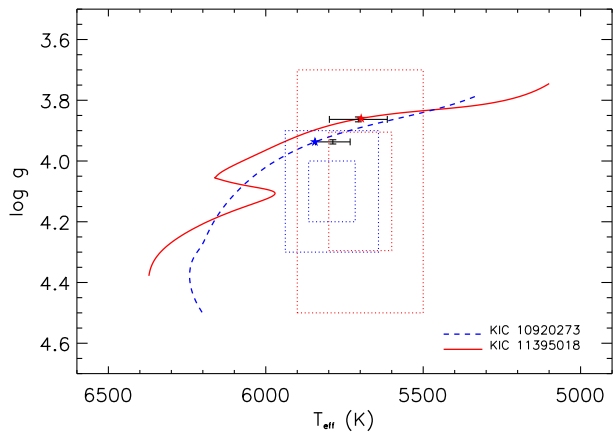


FIG. 1.— $\log g$ - T_{eff} diagram for KIC 10920273 and KIC 11395018. Surface gravity, g , is in cgs units. Spectroscopic constraints given in Table 1 are shown by 1- and 2- σ error boxes (dotted; blue for KIC 10920273 and red for KIC 11395018). Evolutionary tracks of two models indicated by star symbols (SA1 and BA1 from Tables 4 and 5) are plotted using the same color code. The points with error bars represent the weighted means and the standard deviations of the asteroseismic determinations (see Tables 4 and 5).

2.2. Asteroseismic data

We used *Kepler* data from observations made in the period from 2009 May to 2010 March, i.e., from the commissioning run (Q0) through Quarter 4 (Q4). The formal frequency resolution is $\sim 0.05 \mu\text{Hz}$. From the power spectra, Campante et al. (2011) and Mathur et al. (2011) reported individual frequencies for KIC 10920273 and KIC 11395018, based on analyses performed by several teams. The final sets of results included a minimal and a maximal list of frequencies, where the former were those agreed upon by more than half of the fitters and the latter were those agreed upon by at least two fitters. Therefore, the frequencies that are in the maximal list but not the minimal list are less certain. For details of the frequency-extraction techniques and the selection methods, we refer the reader to Campante et al. (2011) and Mathur et al. (2011). The analysis of each star resulted in the extraction of up to a total of 25 individual oscillation frequencies for radial ($l = 0$), dipole ($l = 1$), and quadrupole ($l = 2$) modes, including several mixed modes. These mixed modes carry information from the core and hence provide stronger constraints on the evolutionary stage of the stars, as discussed in Section 1. We started by searching for models using the minimal-list of frequencies and then extended our analysis to include additional frequencies from the maximal lists.

3. MODELING APPROACH

Asteroseismic modeling is performed by optimizing the stellar model parameters to match the observed seismic quantities and also the classically observed (or derived) stellar properties, such as effective temperature, surface gravity, surface metallicity (along with radius, mass and luminosity, when available). The seismic quantities include, but are not limited to, the average large and small frequency separations², the frequency of maximum power in the oscillation spectrum (ν_{max}), and the individual oscillation frequencies. Naturally, the individual frequencies provide the most detailed information and the highest precision in the derived stellar properties (see, e.g., Metcalfe et al. 2010 and Mathur et al. 2012).

We used the individual oscillation frequencies and the atmospheric properties (T_{eff} , $\log g$, and [Fe/H]) as constraints to carry out the stellar model optimization. As an initial guess for the parameter space to be searched, we used preliminary results of the mass determination from the analysis of Creevey et al. (2012), which were in agreement with their final results within the uncertainties. They derived stellar properties using the average seismic quantities together with the atmospheric constraints. The final values given by Creevey et al. (2012) were $1.25 \pm 0.13 M_{\odot}$ for KIC 10920273 and $1.37 \pm 0.11 M_{\odot}$ for KIC 11395018.

Five teams participated in the modeling of these stars using a variety of evolutionary codes and fitting methods. Most of the methods were either based on searching for the best-fitting model in a grid specifically computed for this analysis or on using a pre-existing grid to determine the general area of the stellar properties in the param-

² The large frequency separation is $\Delta\nu_{n,l} = \nu_{n,l} - \nu_{n-1,l}$, and the small frequency separation is $\delta\nu_{n,l} = \nu_{n,l} - \nu_{n-1,l+2}$, where $\nu_{n,l}$ is the frequency of the mode with spherical degree l and radial order n .

ter space before going into further refinement process for individual stars. One team used the Asteroseismic Modeling Portal (AMP), which is a pipeline analysis tool that optimizes the seismic and non-seismic properties globally using a genetic algorithm. AMP starts the model-search with four random independent sets of initial parameters and performs the search over a large parameter space (Metcalf et al. 2009; Woitaszek et al. 2009). The variety of codes and methods employed give us an estimate of the external uncertainties inherent in the analysis. The list of codes and the configurations regarding the input physics are presented in Table 2.

The individual fitting methods also differed slightly. ASTEC1 calculated grids of models within the $3\text{-}\sigma$ uncertainty of the non-seismic constraints and performed the optimization by a 2-step process, refining the grids several times in the second step guided by the seismic χ^2 values – described by Equation (3). ASTEC2 explored the models, which included turbulent diffusion, and calculated individual models guided by the frequencies. CESAM looked for models reproducing the first avoided crossing as an initial requirement and then performed an optimization using χ^2 -minimization to determine stellar mass and age (see Deheuvels & Michel 2011 for details of this method). The Geneva stellar evolution code was used to compute grids of rotating models with an initial velocity of 50 km s^{-1} on the zero-age main sequence (ZAMS). This value results in surface velocities that are typically lower than 10 km s^{-1} at the end of the main sequence (MS) for a solar-type star that is assumed to undergo magnetic braking on the MS due to the presence of a convective envelope (Krishnamurthi et al. 1997). The initial parameters used by each team are given in Table 3.

Oscillation frequencies of low-degree modes were calculated by LOSC (Scuflaire et al. 2008) for stellar models computed by CESAM, while the Aarhus Adiabatic Pulsation Package (ADIPLS, Christensen-Dalsgaard 2008b) was used to calculate the frequencies for all of the other models.

In relation to the oscillation frequencies, there is a well-known offset between the observed and the model frequencies for the Sun and solar-type stars, due to inaccurate representation of the near-surface layers in the models. To address this issue, we used the empirical correction suggested by Kjeldsen et al. (2008), who showed that the difference between the observed and calculated solar frequencies, which gets larger with increasing frequency, can be fitted by a power law:

$$\nu_{\text{obs}}(n, 0) - \nu_{\text{best}}(n, 0) = a \left(\frac{\nu_{\text{obs}}(n, 0)}{\nu_0} \right)^b, \quad (1)$$

where $\nu_{\text{obs}}(n, 0)$ and $\nu_{\text{best}}(n, 0)$ are the observed and best model frequencies with degree $l = 0$ and radial order n , ν_0 is a constant frequency usually chosen to be the frequency at maximum oscillation power, a is the size of the correction at ν_0 and can be calculated for each model, and b is the exponent to be determined.

The right-hand-side of Equation (1) is the correction term to be added to the acoustic (p-mode) frequencies of the best models. The mixed modes, however, are less sensitive to the properties of the near-surface layers since much of their energy is confined to the stellar center. In

other words, we need to apply a smaller near-surface correction to the frequency of a mixed mode than to a p mode with a similar frequency. Following Brandão et al. (2011), we scaled the magnitude of the correction inversely with Q_{nl} , the inertia of a given mode normalized by the inertia of a radial ($l = 0$) mode at the same frequency (see, e.g., Aerts et al. 2010). Note that the inertia of a mixed mode is much higher than that of a p mode. The correction to be applied to all calculated frequencies is then of the form:

$$\nu_{\text{corr}}(n, l) = \nu_{\text{best}}(n, l) + a \left(\frac{1}{Q_{nl}} \right) \left(\frac{\nu_{\text{best}}(n, l)}{\nu_0} \right)^b, \quad (2)$$

where ν_{corr} represents the corrected model frequencies. Notice that $\nu_{\text{obs}}(n, 0)$ on the right-hand-side of Equation (1) is replaced by the best model frequencies in order to allow us to correct the frequencies outside the range of observed radial modes (see, Brandão et al. 2011, for details).

The solar value of the exponent b was calculated by Kjeldsen et al. (2008) to be 4.90 using the GOLF data (Lazrek et al. 1997) and the solar “Model S” of Christensen-Dalsgaard et al. (1996). This value was found to range from 4.40 to 5.25 for the same model, depending on the number of radial orders included in the calibration, but a was found to vary by less than $0.1 \mu\text{Hz}$ in all cases. Kjeldsen et al. (2008) suggested that the solar b value may be used for solar-like stars and this approach was successfully applied to β Hyi (Brandão et al. 2011), HD 49385 (Deheuvels & Michel 2011), KIC 11026764 (Metcalf et al. 2010) and a sample of *Kepler* stars (Mathur et al. 2012). In this work ASTEC1, ASTEC2, and Geneva codes adopted the solar value $b = 4.90$ from Kjeldsen et al. (2008) for calculating the correction term, while AMP adopted $b = 4.82$, which is the solar-calibrated value for AMP with the BiSON data (Chaplin et al. 1999), and CESAM adopted $b = 4.25$, the calibrated value using the GOLF data (Gelly et al. 2002). Given how little a varies for a relatively large range of b for a given model, as discussed above, using slightly different b values for model-fitting has a negligible impact on the results.

4. RESULTS AND DISCUSSION

4.1. Global properties

To select the best models, we defined the two normalized χ^2 measures shown in Equations (3) and (4), which allowed us to evaluate the qualities of the fits for the atmospheric parameters and the seismic parameters separately. The seismic measure was

$$\chi_{\text{seis}}^2 = \frac{1}{N} \sum_{n,l} \left(\frac{\nu_{\text{obs}}(n, l) - \nu_{\text{corr}}(n, l)}{\sigma(\nu_{\text{obs}}(n, l))} \right)^2, \quad (3)$$

where N is the number of observed frequencies, $\nu_{\text{corr}}(n, l)$ represents the near-surface-corrected model frequencies with spherical degree l and radial order n , $\nu_{\text{obs}}(n, l)$ are the observed frequencies, and $\sigma(\nu_{\text{obs}}(n, l))$ are the uncertainties on the observed frequencies. The measure for the atmospheric properties was

$$\chi_{\text{atm}}^2 = \frac{1}{3} \sum \left(\frac{P_{\text{obs}} - P_{\text{mod}}}{\sigma(P_{\text{obs}})} \right)^2, \quad (4)$$

where $P = \{T_{\text{eff}}, \log g, [\text{Fe}/\text{H}]\}$ and the subscripts “obs” and “mod” represent the observed and model properties, respectively, with $\sigma(P_{\text{obs}})$ denoting the observational uncertainties. The values of $[\text{Fe}/\text{H}]$ for the models were calculated using the formula $[\text{Fe}/\text{H}] = \log(Z/X)_{\text{mod}} - \log(Z/X)_{\odot}$, where the solar value was adopted from Grevesse & Noels (1993) as $(Z/X)_{\odot} = 0.0245$.

Each modeling team returned the model that best matched the observational constraints. We present the properties of these models in Tables 4 and 5, along with the normalized χ^2 values³. We also present models fitted using more or fewer frequencies than those in the minimal lists in order to see whether the model-fitting results change considerably. In each case, we calculated the χ^2_{seis} in the tables using only the frequencies that were common constraints for all of the models, in order to achieve a consistent evaluation of the models.

There is a good agreement between the observed frequencies and the model frequencies. The quality of the fits can be seen in the échelle diagrams for a sample of models (Fig. 2). Overall frequency patterns, including the dipolar mixed modes, are matched quite well. The fact that $\chi^2_{\text{seis}} > 1.0$ implies that either the observational uncertainties are underestimated or the models are incomplete representations of the observational data. The models with relatively high $\chi^2_{\text{seis}} (\gtrsim 20.0)$, are those that either could be improved with further refinement or that do not reproduce all of the modes simultaneously, in particular the mixed modes, which are more difficult to fit. Due to their strong sensitivity to stellar evolution, mixed modes tend to dominate the model-fitting results. The timescale on which the signatures of these modes evolve is very short, so it becomes difficult to find good fits unless the grid of models used is very fine.

We present our results in Tables 4 and 5. Properties of all the models are listed, along with the weighted mean values and the standard deviations. Both stars have left the main sequence (central hydrogen mass fraction $X_c = 0.0$) but have quite different characteristics, as seen in Tables 4 and 5. The fact that KIC 10920273 is an old solar analog (with one solar mass and near-solar metallicity) makes it an interesting target for further studies. A typical solar model would turn off from the MS at around 9–10 Gyr. However, the metallicity and particularly the helium abundance alter this age estimate. In this case it is the high helium abundance that affects the MS turn-off age more than the low metallicity. The models with higher helium abundance behave similar to those with higher mass (higher luminosity), following an evolutionary track similar to that of a higher-mass star, and hence have shorter MS lifetimes.

The results in Tables 4 and 5 were weighted by the goodness of the seismic fit, i.e. the inverse of χ^2_{seis} . This way, any misleading contribution due to coarse grids is eliminated. Although this does not provide a direct measurement of the systematic uncertainties, it still allows us to estimate the order of magnitude of the external errors expected from using different inputs, codes, and fitting methods. A similar determination of the systematic er-

rors for the case of bright *Kepler* stars 16 Cyg A and B was carried out by Metcalfe et al. (2012) using different evolutionary codes and fitting methods. The uncertainties we determined are mostly greater due to the lower SNR in the data of our faint stars. Systematic errors in determination of stellar properties using grid-based pipelines caused by different observational constraints and different input physics were discussed more generally for a few *Kepler* stars by Creevey et al. (2012). We discuss the uncertainties further in the next section.

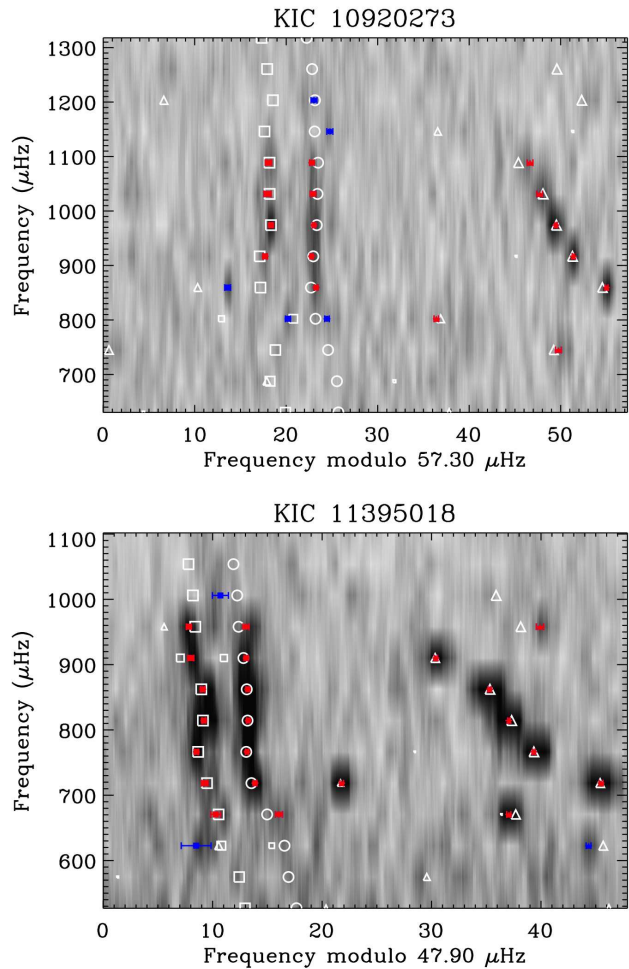


FIG. 2.— Échelle diagrams for the selected models of KIC 10920273 (SA3, upper panel) and KIC 11395018 (BD, lower panel). The radial orders are plotted horizontally (see Bedding 2012) and the vertical axes indicate the frequencies at the middle of each order. The background is a gray-scale map of the power spectrum from the observations, with the observed frequencies shown by filled symbols with $1\text{-}\sigma$ error bars. Minimal-list frequencies are plotted in red, while the additional maximal-list frequencies are plotted in blue. Open symbols are used for the model frequencies, with smaller size implying larger normalized mode inertia. Circles, triangles, and squares represent $l = 0$, $l = 1$, and $l = 2$ modes respectively.

4.2. Discussion of uncertainties

To evaluate the typical uncertainties caused by different input physics further, we calculated some additional models and small grids using KIC 10920273 as a

³ The labels of the models presented in Tables 4 and 5 start with “S” and “B” for KIC 10920273 and KIC 11395018, which stand for “Scully” and “Boogie” – the nicknames of the stars within Kepler Asteroseismic Science Consortium, Working Group 1.

test case. We selected SB1 as our base model. Keeping the input parameters (mass, Z/X , Y , α) fixed, we first explored the effects of changing one single ingredient of input physics at a time. We also changed the value of α while keeping everything else fixed. On every new evolutionary sequence, we calculated the frequencies of the models that had all atmospheric properties ($\log g$, T_{eff} , and $[\text{Fe}/\text{H}]$) within 3σ of the observed values. We then selected the model that best matched the observed frequencies. In the cases of including core overshoot, changing the convection treatment (to CGM formulation), and using several different nuclear rates (Bahcall et al. 1995; Parker 1986; Adelberger et al. 1998), the new models reproduced the observed frequencies as well as the base model with an age difference of only 0.7% at most (which corresponds to changes in radius of $<0.2\%$ and in $\log g$ of $<0.1\%$). This means that the uncertainties on the final parameters caused by the corresponding inputs were negligible. We note that the effect of core overshoot would be more significant for a main-sequence star.

For the cases where we did not obtain a model having a seismic χ^2 comparable to that of the base model, we carried on with the analysis. These cases resulted from including diffusion and gravitational settling of helium, using two different versions of the low-temperature opacities given in Table 2, and varying the value of mixing length parameter (in the range of 1.6–2.0). For each of these cases, we computed additional small grids around the base model by varying all the input parameters, in order to see how much the output properties were different for two models with different input physics but similar frequencies. We then calculated the weighted mean and standard deviation in the same way as in the original analysis. The standard deviation in this case represents the typical uncertainties caused by using a fixed set of input physics, hence decreasing the level of model-dependence in the results substantially. The mean values for age, luminosity, radius, T_{eff} , and $\log g$ calculated from the additional analysis agreed with the original results within 1σ , while their standard deviations were of the same order as those given in Table 4. This confirms that the uncertainties presented here are realistic. Moreover, the resulting values of radius and $\log g$ from the additional analysis are essentially the same as the original results. This is reassuring given the importance of asteroseismology in determining the radius in a robust way.

The internal uncertainties were different for each method. However, the dominant source of uncertainty is the non-uniqueness of the solution rather than the statistical errors. Parameter correlations allow a trade-off between parameters, leading to different families of solutions that are almost equally good seismic fits. The effective range of these correlations is narrowed substantially, but not eliminated, by the use of seismic data. We used a single method (AMP) to evaluate the uniqueness of the best models for both stars, since the uniqueness depends on the specific constraints adopted in each case. AMP finds the lowest value of χ^2 in the entire search space. Along the way it also identifies the secondary minima – which can be far away from, but not much worse than, the formally best solution. For both stars, these secondary minima (SA2 and BA2 in Tables 4 and 5) are marginally worse than the best solutions found using

the same set of inputs (SA1 and BA1), but the values of the mass and helium abundance are quite different. This reflects the well-known mass-He degeneracy (see, e.g., Lebreton et al. 1993; Fernandes & Monteiro 2003; Metcalfe et al. 2009), which is not entirely lifted, even with the help of asteroseismology. The mass is constrained more strongly than it would be without asteroseismic data but in the absence of external constraints on the helium abundance, we cannot choose one particular model. Consequently, we used both the primary and secondary-minimum solutions from AMP in the calculation of the weighted means. The range of the AMP results leads to relatively large “uniqueness uncertainties” in the fitted stellar properties. These are determined as follows for KIC 10920273, and KIC 11395018, respectively: 3%, and 7% in stellar mass; 8%, and 21% in the initial metallicity (Z/X); 10%, and 25% in Y_i ; 7%, and 8% in age; and 1%, and 2% in radius. Note that the larger uncertainties in the mass and chemical composition for KIC 11395018 reflect the fact that it has *two* observed avoided crossings, which provide more stringent constraints such that neighboring models are significantly worse. Only a relatively large jump along the parameter correlations yielded a secondary minimum with a comparable seismic fit (cf. Metcalfe et al. 2010). When we evaluate the uncorrelated statistical uncertainties for each of these minima with a local analysis using singular value decomposition (SVD), we found very small errors (e.g., as low as $5 \times 10^{-3}\%$ for mass), reflecting the steep χ^2 surfaces corresponding to these results. Although these ‘local’ uncertainties are real, i.e., changing the values of the parameters by the correlated ‘tiny’ uncertainties causes a large increase in the χ^2 (>50), the minima are not unique. Hence, a local analysis does not reflect the true uncertainties of the overall results.

Inclusion of the maximal list of frequencies as constraints in the analysis (five additional frequencies for KIC 10920273 and two for KIC 11395018) made the agreement between the model and observations better for both KIC 10920273 (SA3 in Table 4) and KIC 11395018 (see BA3 in Table 5). We also used a third list for KIC 10920273 to ensure that the less-certain frequencies did not bias our model-fitting. For that purpose, we left out two frequencies in the analysis. One of these was identified as a dipole-mode frequency belonging to the minimal list, but tagged as being close to the second harmonic of the long-cadence frequency (with $\nu = 1135.36 \pm 0.31 \mu\text{Hz}$), while the other one was identified as a quadrupole mode (with $\nu = 873.10 \pm 0.32 \mu\text{Hz}$) that was tagged as a possible mixed mode introduced a posteriori (Campante et al. 2011). Both SA4 and SB2 were selected using this alternative frequency set for KIC 10920273, and the agreement between the model and observations was not affected substantially. Therefore, we cannot ascertain whether these two peaks are stellar in origin. Nevertheless, we do not completely rule out the possibility of these peaks being stellar as some of the models that result from using alternative frequency sets do contribute to the weighted mean values significantly. Furthermore, we note that the peak at $\nu = 873.10 \mu\text{Hz}$, which is tagged as a possible quadrupole mixed mode, is in the middle of the frequencies of a dipole mixed mode and a quadrupole mode in most of our models. So the

observed peak may correspond to a dipole mixed mode, which, according to the models, has a relatively low normalized mode inertia indicating an observable amplitude.

4.3. Comparison with previous results

Comparing our results with those from the pipeline analyses of Creevey et al. (also given here in Tables 4 and 5), we see that the mass determinations from the pipeline analyses were higher, which led to lower age estimates. We emphasize that the previous pipeline analyses used only the average seismic quantities, hence lacking additional information from the individual frequencies and being affected by the uncertainties of the scaling relations. Therefore, some deviation from their values was expected. Nonetheless, it is reassuring that the mass, radius, and age determinations of Creevey et al. (2012) are within $2\text{-}\sigma$ uncertainty limits of our results for KIC 10920273, and within 1σ for KIC 11395018. We also confirm the robust determination of $\log g$ using scaling relations and grid-based analyses (see Table 7 in Creevey et al. 2012), with which our results are in agreement within 1σ . Additionally, we note that our results confirm that the mass and radius determined using only the scaling relations (e.g., Mathur et al. 2012) provide good initial estimates for these properties ($1.06 \pm 0.20 M_{\odot}$ and $1.80 \pm 0.11 R_{\odot}$ for KIC 10920273; $1.31 \pm 0.25 M_{\odot}$ and $2.21 \pm 0.14 R_{\odot}$ for KIC 11395018).

There is excellent agreement, for both stars, between our results and the mass estimates of Benomar et al. (2012), who used the coupling strength of the observed mixed modes to determine the masses of several subgiants, including KIC 10920273 ($1.04 \pm 0.04 (\pm 0.04) M_{\odot}$) and KIC 11395018 ($1.21 \pm 0.06 (\pm 0.04) M_{\odot}$).

The most substantial improvement in this work comes from the use of individual frequencies which yield increased precision, with age being affected the most. The presence of the mixed modes in the data allowed us to determine the age with 5-7% precision, although with some model-dependency. This result is a major improvement on the 35-40% precision in age achieved using atmospheric and mean seismic parameters. Both stars are determined to be post-main-sequence subgiants with no hydrogen left in their cores. Evolutionary tracks of the selected models are shown in Fig. 1.

Although we did not restrict the parameter search to be within $1\text{-}\sigma$ uncertainty around the spectroscopic constraints, the weighted mean values of T_{eff} from the models are within $1\text{-}\sigma$ limit for both stars, while $\log g$ results are in agreement with the spectroscopic values within 2σ (see Fig. 1), and $[\text{Fe}/\text{H}]$ within 1.5σ . Our $\log g$ results are in excellent agreement with asteroseismic $\log g$ values obtained from scaling relations (given by Creevey et al. (2012) and also in Tables 4 and 5). We also note that our temperature results are in good agreement with the revised photometric values for the Kepler Input Catalog (KIC) from Pinsonneault et al. (2012), who derived $T_{\text{eff}} = 5872 \pm 70$ K for KIC 10920273, and $T_{\text{eff}} = 5650 \pm 59$ K for KIC 11395018.

4.4. Non-seismic age diagnostics

We discussed the asteroseismic constraints on the stellar age in Section 1. Here we discuss the implications of rotation and stellar activity on the age, as well as those of the surface lithium abundance.

Rotation and activity are potentially valuable diagnostics of stellar age. It was shown that the Ca^+ emission luminosity, an indicator of stellar activity, decays roughly as $t^{-0.5}$ for some cluster stars and the Sun (Skumanich 1972), furthermore, rotational decay was shown to follow the same law. Large samples of stellar rotation periods have been collected, and the *Kepler* mission promises many more. There is therefore substantial interest in stellar rotation-mass-age, or gyrochronology, relations (see Barnes 2003, 2007; Mamajek & Hillenbrand 2008; Meibom et al. 2011; Epstein & Pinsonneault 2012). We discussed in Section 2.1 that relatively slow rotation is inferred for both stars. Slow rotation rates imply relatively old stars, which is consistent with our asteroseismic determinations. However, one would not expect main-sequence spin-down relationships to apply directly to the evolved stars. Therefore, we cannot use the rotation rates for these stars to infer their ages with the age-rotation relations established for MS stars; these relations need to be calibrated for more evolved stars using larger samples.

We have analyzed the chromospheric activity in the CaII HK lines and found the levels of activity in both stars to be very low. Fig. 3 shows the CaII K and H lines of KIC 10920273 and KIC 11395018 compared to the Sun. The solar spectrum was obtained from the solar light reflected by Ganymede, which was observed with HARPS in April 2007⁴, when the Sun was close to the minimum of its activity cycle. We accounted for the different resolving power of HARPS ($R \simeq 120,000$) compared to FIES spectrograph ($R \simeq 46,000$) by convolving the solar spectrum with a Gaussian kernel of the appropriate width. It is clear that these two *Kepler* stars have chromospheric activity levels comparable to the quiet Sun, or lower. These low activity levels are consistent with the old ages we infer from asteroseismology; however, the rough nature of the empirical age-activity relations for post-MS stars does not allow us to make a quantitative analysis to infer ages.

Another independent determination of stellar age may be obtained by measuring the Li content at the stellar surface. Lithium is easily destroyed in stellar interiors and is only produced under unusual circumstances; it has therefore been employed as an age indicator for low-mass stars. Lithium can be directly depleted if the surface convection zone is deep enough. It can also be mixed into the radiative interior, or it can be stored below the surface convection zone by microscopic diffusion processes. In standard stellar models, pre-main-sequence depletion occurs for most low-mass stars when they have deep convection zones, and it is most severe in lower mass stars (Bodenheimer 1965). In a qualitative sense, a detection of Li in very cool stars is a strong indicator of youth. However, standard models also predict that stars of order 0.9 solar masses and higher would not experience main-sequence Li depletion, and there is strong evidence from open clusters for a steady decrease in Li as a function of time, even for stars more massive than the Sun (see Zappala 1972; Pinsonneault 1997; and Sestito & Randich 2005 for reviews.)

It was also shown by Randich (2010) that, for a fraction

⁴ <http://www.eso.org/sci/facilities/lasilla/instruments/harps/inst/monitoring/sun.html>

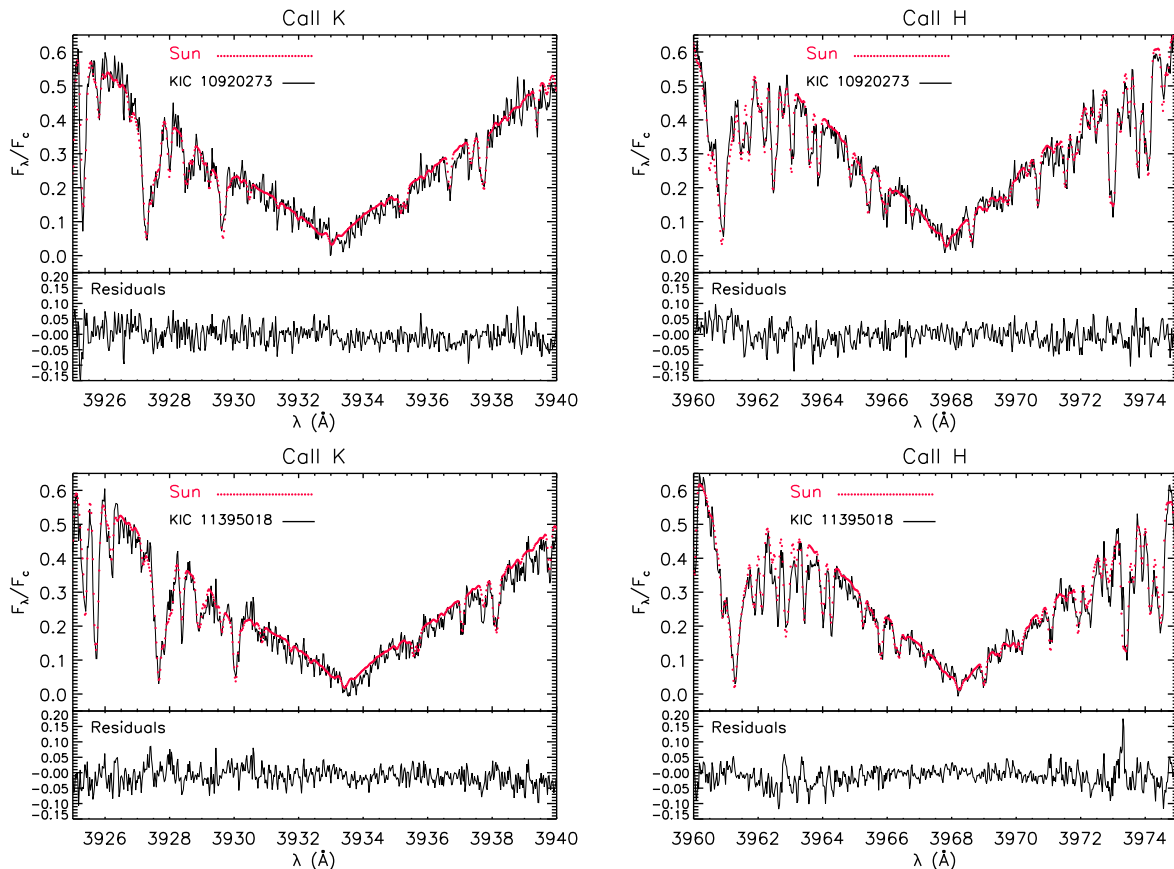


FIG. 3.— Chromospheric activity in the CaII K and CaII H lines (flux relative to the continuum) for KIC 10920273 (upper panels) and KIC 11395018 (lower panels). The solar spectrum (Ganymede taken in 2007 with HARPS) is overplotted with a dotted (red) line. The residuals between the stellar and solar spectra (at the bottom of each plot) show that the two stars have activity levels comparable to the quiet Sun or lower.

of solar-like stars with effective temperatures between 5750 K and 6050 K, Li is not further depleted after the age of ~ 1 Gyr, unlike for the Sun and many other stars. Due to this bimodal pattern, Li abundance alone cannot be used to determine the age for all stars, and a high Li abundance can only help define a lower limit for the age, since it may correspond either to a young star that has not yet depleted much Li, or to an older star that has stopped depleting Li a long time ago.

Creevey et al. (2012) showed that the two stars considered here have strong Li absorption lines, which implies a high Li content at the surface ($\log N(\text{Li}) = 2.4 \pm 0.1$ for KIC 10920273 and $\log N(\text{Li}) = 2.6 \pm 0.1$ for KIC 11395018; where $\log N(\text{Li}) = \log [n(\text{Li})/n(\text{H})] + 12$, with n being the number density of atoms and $\log N(\text{H}) = 12$ by definition). Considering the empirical Li-age relation established by Sestito & Randich (2005), Creevey et al. then determined that the given Li abundances would indicate low ages (1-3 Gyr for KIC 10920273 and 0.1-0.4 Gyr for KIC 11395018), which are incompatible with the asteroseismic ages they determined through the pipeline modeling (see Tables 4 and 5) performed using the average asteroseismic quantities.

However, in addition to the bi-modality mentioned above, the age-Li relation has been shown to be valid for MS stars and does not necessarily extend to more evolved stars. This makes the age determination using

the Li abundance ambiguous. Thus, despite the high Li abundance, we are confident that these are indeed evolved stars that have left the main sequence, due to the presence of the mixed modes in the observed oscillation spectra and as confirmed by our asteroseismic analysis.

5. SUMMARY AND CONCLUSIONS

We performed asteroseismic modeling of two *Kepler* stars, KIC 10920273 and KIC 11395018, for which we have long seismic data sets (>8 months) and ground-based follow-up spectra. We used individual oscillation frequencies and atmospheric properties as initial constraints. We employed several evolutionary codes with different input physics, and various fitting methods to determine the global stellar properties and estimate their uncertainties (see Tables 4 and 5). The near-surface correction was applied to the models, which reproduced the individual observed frequencies with considerable success; see Fig. 2 for a qualitative representation with échelle diagrams. These two relatively faint stars, which have similar atmospheric properties according to the ground-based data, turned out to be substantially different – more than could have been predicted from their different metallicities – after incorporating the high-precision asteroseismic data into the modeling.

KIC 10920273 resembles an old Sun, having one solar mass ($1.00 \pm 0.04 M_{\odot}$) and an age of $\tau = 7.12 \pm 0.47$ Gyr, while KIC 11395018 has a mass of $1.27 \pm 0.04 M_{\odot}$ and an

age very close to that of the Sun ($\tau = 4.57 \pm 0.23$ Gyr). These results agree, at the $2\text{-}\sigma$ level for KIC 10920273 and $1\text{-}\sigma$ level for KIC 11395018, with the properties determined using the average asteroseismic quantities. The results presented here are much more precise than those from the average asteroseismic quantities, though, and they are also more accurate as a result of using more observational information, i.e. individual frequencies, and stronger constraints extracted from the observations, such as the mixed modes. We confirm the robust determination of $\log g$ from the average seismic quantities, as our results are within $1\text{-}\sigma$ uncertainty of the pipeline results.

We confirmed these stars to be subgiants (having evolved off the main sequence) and this allowed us to resolve the disagreement between the seismic ages determined from the pipeline analyses and the ages estimated using the lithium abundance and the empirical Li-age relationship. Basically, the Li abundance cannot be employed to estimate the ages of the subgiants. Similarly, existing age-rotation-activity relations can only be indicative for subgiants as these relations are calibrated mostly for the main-sequence stars. This must be taken into account for gyrochronology studies.

We will soon obtain longer data sets from *Kepler* for many more stars and our results are a good indication of what we can achieve. We note that KIC 10920273 and KIC 11395018 are at the faint end of the *Kepler* asteroseismic targets; hence, this work sets a lower limit to the quality of information we can expect from asteroseismology.

We thank the entire *Kepler* team, without whom these results would not be possible. Funding for this Discovery mission is pro-

vided by NASA's Science Mission Directorate. We also thank all funding councils and agencies that have supported the activities of KASC Working Group 1. This article is based on observations made with the Nordic Optical Telescope (NOT) operated on the island of La Palma in the Spanish Observatorio del Roque de los Muchachos. GD gratefully acknowledges financial support from the following institutions: Advanced Study Program (ASP) of the National Center for Atmospheric Research (NCAR), NASA under Grant No. NNX11AE04G (together with MP and TSM), The Danish Council for Independent Research; and thanks Y. Elsworth, S. Hekker, M. Stęślicki, J. C. Suárez, M. J. Thompson, and the anonymous referee for useful comments. NCAR is partially supported by the National Science Foundation. Funding for the Stellar Astrophysics Centre is provided by The Danish National Research Foundation. The research is supported in part by the ASTERISK project (ASTERoseismic Investigations with SONG and Kepler) funded by the European Research Council (Grant agreement no.: 267864). AOT acknowledges support from Sonderforschungsbereich SFB 881 "The Milky Way System" (subproject A5) of the German Research Foundation (DFG). IMB is supported by the grant SFRH / BD / 41213 /2007 from FCT /MCTES, Portugal. IMB and MJPG were supported in part by grant PTDC/CITE-AST/098754/2008 from FCT-Portugal and FEDER. JM-Ż acknowledges the Polish Ministry grant number NN203 405139. KB acknowledges the funding support from the INAF Postdoctoral fellowship. This research was carried out while OLC was a Henri Poincaré Fellow at the Observatoire de la Côte d'Azur. The Henri Poincaré Fellowship is funded by the Conseil Général des Alpes-Maritimes and the Observatoire de la Côte d'Azur. RAG has received funding from the European Community's Seventh Framework Programme (FP7/2007-2013) under grant agreement No. 269194 (IRSES/ASK). SGS acknowledges the support from the Fundação para a Ciência e Tecnologia (grant ref. SFRH/BPD/47611/2008) and the European Research Council (grant ref. ERC-2009-StG-239953). TLC acknowledges financial support from project PTDC/CITE-AST/098754/2008 funded by FCT/MCTES, Portugal. WJC acknowledges financial support from the UK Science and Technology Facilities Council. We acknowledge the KITP staff at UCSB for their warm hospitality during the research program "Asteroseismology in the Space Age". This research was supported in part by the National Science Foundation under Grant No. PHY05-51164.

REFERENCES

- Adelberger, E. G., Austin, S. M., Bahcall, J. N., et al. 1998, *Reviews of Modern Physics*, 70, 1265
- Aerts, C., Christensen-Dalsgaard, J., & Kurtz, D. W. 2010, *Asteroseismology*, Springer, Heidelberg (Springer, Heidelberg)
- Aizenman, M., Smeyers, P., & Weigert, A. 1977, *A&A*, 58, 41
- Alexander, D. R. & Ferguson, J. W. 1994, *ApJ*, 437, 879
- Angulo, C., Arnould, M., Rayet, M., et al. 1999, *Nuclear Physics A*, 656, 3
- Appourchaux, T., Chaplin, W. J., García, R. A., et al. 2012, *A&A*, 543, A54
- Bahcall, J. N. & Pinsonneault, M. H. 1992, *Reviews of Modern Physics*, 64, 885
- Bahcall, J. N., Pinsonneault, M. H., & Wasserburg, G. J. 1995, *Reviews of Modern Physics*, 67, 781
- Barnes, S. A. 2003, *ApJ*, 586, 464
- Barnes, S. A. 2007, *ApJ*, 669, 1167
- Bedding, T. R. 2012, in *Astronomical Society of the Pacific Conference Series*, Vol. 462, *Progress in Solar/Stellar Physics with Helio- and Asteroseismology*, ed. H. Shibahashi, M. Takata, & A. E. Lynas-Gray, 195
- Benomar, O., Bedding, T. R., Stello, D., et al. 2012, *ApJ*, 745, L33
- Bodenheimer, P. 1965, *ApJ*, 142, 451
- Böhm-Vitense, E. 1958, *Zeitschrift für Astrophysik*, 46, 108
- Borucki, W. J., Koch, D., Basri, G., et al. 2010, *Science*, 327, 977
- Brandão, I. M., Doğan, G., Christensen-Dalsgaard, J., et al. 2011, *A&A*, 527, A37
- Campante, T. L., Handberg, R., Mathur, S., et al. 2011, *A&A*, 534, A6
- Canuto, V. M., Goldman, I., & Mazzitelli, I. 1996, *ApJ*, 473, 550
- Chaplin, W. J., Appourchaux, T., Elsworth, Y., et al. 2010, *ApJ*, 713, L169
- Chaplin, W. J., Elsworth, Y., Isaak, G. R., Miller, B. A., & New, R. 1999, *MNRAS*, 308, 424
- Chaplin, W. J., Kjeldsen, H., Christensen-Dalsgaard, J., et al. 2011, *Science*, 332, 213
- Christensen-Dalsgaard, J. 2008a, *Ap&SS*, 316, 13
- Christensen-Dalsgaard, J. 2008b, *Ap&SS*, 316, 113
- Christensen-Dalsgaard, J., Dappen, W., Ajukov, S. V., et al. 1996, *Science*, 272, 1286
- Creevey, O. L., Doğan, G., Frasca, A., et al. 2012, *A&A*, 537, A111
- Deheuvels, S., García, R. A., Chaplin, W. J., et al. 2012, *ApJ*, 756, 19
- Deheuvels, S. & Michel, E. 2011, *A&A*, 535, A91
- Eggenberger, P., Meynet, G., Maeder, A., et al. 2008, *Ap&SS*, 316, 43
- Eggenberger, P., Meynet, G., Maeder, A., et al. 2010, *A&A*, 519, A116
- Epstein, C. R. & Pinsonneault, M. H. 2012, arXiv:1203.1618; submitted to *ApJ*
- Ferguson, J. W., Alexander, D. R., Allard, F., et al. 2005, *ApJ*, 623, 585
- Fernandes, J. & Monteiro, M. J. P. F. G. 2003, *A&A*, 399, 243
- Frandsen, S. & Lindberg, B. 1999, in *Astrophysics with the NOT*, ed. H. Karttunen & V. Pirola, 71
- Gelly, B., Lazrek, M., Grec, G., et al. 2002, *A&A*, 394, 285
- Gilliland, R. L., Jenkins, J. M., Borucki, W. J., et al. 2010, *ApJ*, 713, L160
- Grevesse, N. & Noels, A. 1993, in *Origin and Evolution of the Elements*, ed. S. Kubono & T. Kajino, 14
- Iglesias, C. A. & Rogers, F. J. 1996, *ApJ*, 464, 943
- Kjeldsen, H., Bedding, T. R., & Christensen-Dalsgaard, J. 2008, *ApJ*, 683, L175
- Koch, D. G., Borucki, W. J., Basri, G., et al. 2010, *ApJ*, 713, L79

- Krishnamurthi, A., Pinsonneault, M. H., Barnes, S., & Sofia, S. 1997, *ApJ*, 480, 303
- Lazrek, M., Baudin, F., Bertello, L., et al. 1997, *Sol. Phys.*, 175, 227
- Lebreton, Y., Auvergne, M., Morel, P. J., & Baglin, A. 1993, in *Astronomical Society of the Pacific Conference Series*, Vol. 40, IAU Colloq. 137: Inside the Stars, ed. W. W. Weiss & A. Baglin, 474
- Mamajek, E. E. & Hillenbrand, L. A. 2008, *ApJ*, 687, 1264
- Mathur, S., Handberg, R., Campante, T. L., et al. 2011, *ApJ*, 733, 95
- Mathur, S., Metcalfe, T. S., Woitaszek, M., et al. 2012, *ApJ*, 749, 152
- Meibom, S., Mathieu, R. D., Stassun, K. G., Liebesny, P., & Saar, S. H. 2011, *ApJ*, 733, 115
- Metcalfe, T. S., Chaplin, W. J., Appourchaux, T., et al. 2012, *ApJ*, 748, L10
- Metcalfe, T. S., Creevey, O. L., & Christensen-Dalsgaard, J. 2009, *ApJ*, 699, 373
- Metcalfe, T. S., Monteiro, M. J. P. F. G., Thompson, M. J., et al. 2010, *ApJ*, 723, 1583
- Michaud, G. & Proffitt, C. R. 1993, in *Astronomical Society of the Pacific Conference Series*, Vol. 40, IAU Colloq. 137: Inside the Stars, ed. W. W. Weiss & A. Baglin, 246–259
- Miglio, A., Montalbán, J., & Maceroni, C. 2007, *MNRAS*, 377, 373
- Morel, P. 1997, *A&AS*, 124, 597
- Osaki, J. 1975, *PASJ*, 27, 237
- Parker, P. D. M. 1986, in *Physics of the Sun. Volume 1*, ed. P. A. Sturrock, T. E. Holzer, D. M. Mihalas, & R. K. Ulrich, Vol. 1, 15–32
- Pinsonneault, M. 1997, *ARA&A*, 35, 557
- Pinsonneault, M. H., An, D., Molenda-Żakowicz, J., et al. 2012, *ApJS*, 199, 30
- Pinsonneault, M. H., Kawaler, S. D., & Demarque, P. 1990, *ApJS*, 74, 501
- Proffitt, C. R. & Michaud, G. 1991, *ApJ*, 380, 238
- Randich, S. 2010, in *IAU Symposium*, Vol. 268, IAU Symposium, ed. C. Charbonnel, M. Tosi, F. Primas, & C. Chiappini, 275–283
- Rogers, F. J. & Nayfonov, A. 2002, *ApJ*, 576, 1064
- Scuflaire, R., Montalbán, J., Théado, S., et al. 2008, *Ap&SS*, 316, 149
- Sestito, P. & Randich, S. 2005, *A&A*, 442, 615
- Skumanich, A. 1972, *ApJ*, 171, 565
- Suárez, J. C., Goupil, M. J., Reese, D. R., et al. 2010, *ApJ*, 721, 537
- Woitaszek, M., Metcalfe, T., & Shorrock, I. 2009, in *Proceedings of the 5th Grid Computing Environments Workshop*, p. 1-7
- Zappala, R. R. 1972, *ApJ*, 172, 57

TABLE 2
INPUT PHYSICS USED IN THE EVOLUTION CODES

Team	Diffusion & settling	Convection treatment	Overshoot (core)	EOS	Opacities (high/low temperature)	Nuclear reaction rates
AMP ^a (ASTECC) ^b	He ^c	MLT ^d	no	OPAL2005 ^e	OPAL ^f /Alexander & Ferguson (1994)	B & P (1992) ^g
ASTECC1	none	MLT	no	OPAL2005	OPAL/Ferguson et al. (2005)	NACRE ^h
ASTECC2	He & heavy elements	MLT	no	OPAL2005	OPAL/Ferguson et al. (2005)	NACRE
CESAM ⁱ	none	CGM ^j	yes	OPAL2005	OPAL/Alexander & Ferguson (1994)	NACRE
Geneva ^k	He & heavy elements ^l	MLT	yes	OPAL2005	OPAL/Alexander & Ferguson (1994)	NACRE

a) Metcalfe et al. (2009), b) Aarhus Stellar Evolution Code (Christensen-Dalsgaard 2008a), c) as described by Michaud & Proffitt (1993), d) Mixing length theory (Böhm-Vitense 1958), e) Rogers & Nayfonov (2002), f) Iglesias & Rogers (1996), g) Bahcall & Pinsonneault (1992), h) Angulo et al. (1999), i) Morel (1997), j) Canuto-Goldman-Mazzitelli model for turbulent convection (Canuto et al. 1996), k) Eggenberger et al. (2008) l) Proffitt & Michaud (1991)

TABLE 3
PARAMETER SPACE SEARCHED BY EACH TEAM

Team	M/M _⊙	Z/X	Y	α	α _{ov}
AMP (ASTECC)	0.75–1.75	0.0026–0.079	0.22–0.32	α _{MLT} =1.0–3.0	N/A
ASTECC1	1.00–1.60	0.01–0.07	0.24–0.32	α _{MLT} =1.8	N/A
ASTECC2	1.2–1.4	0.025–0.046	0.26–0.30	α _{MLT} =1.78–1.84	N/A
CESAM	N/A*	0.026–0.042	0.24–0.28	α _{CGM} = 0.52–0.68	0.0–0.2
Geneva	1.00–1.50	0.016–0.040	0.25–0.30	α _{MLT} =1.8	0.1

* For each given set of parameters (Z/X, Y, α, α_{ov}), the method proposed by Deheuvels & Michel (2011) results in a precise estimate of the mass by using the observed large frequency separation and the frequency of the mixed modes.

TABLE 4
FITTED PARAMETERS FOR KIC 10920273.

Model	M/M_{\odot}	$(Z/X)_i$	Y_i	α	$t(\text{Gyr})$	L/L_{\odot}	R/R_{\odot}	$T_{\text{eff}}(\text{K})$	$\log g$	[Fe/H]	X_c	χ_{seis}^2	χ_{atm}^2
SA1 (AMP)	1.00	0.0154	0.296	2.04	6.74	3.31	1.779	5844	3.937	-0.203	0.0	6.33	2.03
SA2 (AMP)	1.03	0.0143	0.267	1.98	7.28	3.24	1.797	5781	3.942	-0.235	0.0	6.35	2.10
SA3 (AMP) ^a	0.96	0.0152	0.311	1.94	6.96	3.14	1.754	5805	3.932	-0.208	0.0	3.09	1.90
SA4 (AMP) ^b	1.00	0.0151	0.285	2.02	6.86	3.22	1.780	5799	3.937	-0.210	0.0	3.60	1.85
SB1 (ASTECC1)	1.02	0.0200	0.290	1.80	7.59	2.97	1.788	5674	3.944	-0.088	0.0	11.44	1.71
SB2 (ASTECC1) ^b	1.06	0.0300	0.300	1.80	7.45	2.84	1.813	5572	3.948	0.088	0.0	23.60	4.21
SC (ASTECC2)	1.10	0.0214	0.285	1.81	5.76	3.42	1.824	5819	3.960	-0.090	0.0	33.90	0.79
SD (CESAM) ^b	0.97	0.0152	0.300	0.56 ^c	7.80	3.10	1.760	5779	3.930	-0.207	0.0	4.00	1.90
SE (Geneva)	1.15	0.0220	0.275	1.80	5.60	3.77	1.861	5900	3.959	-0.040	0.0	45.78	1.40
weighted mean	1.00	0.0161	0.294		7.12	3.18	1.776	5787	3.937	-0.188			
standard deviation	(0.04)	(0.0030)	(0.014)		(0.47)	(0.13)	(0.021)	(55)	(0.007)	(0.064)			
Creevey et al. (2012)	1.25±0.13				4.5±1.8 5.0±1.9 ^d	3.6±1.2	1.90±0.05		3.97±0.03 3.94±0.03 ^e				

^a Maximal-list frequencies are used as input.

^b Two frequencies are excluded from the maximal-list frequencies (see text).

^c Canuto-Goldman-Mazzitelli (CGM) model for turbulent convection (Canuto et al. 1996) is used in this model.

^d This is the value when the average small frequency separation is also used as a seismic constraint.

^e Asteroseismic $\log g$ obtained from scaling relations (Table 7 of Creevey et al. 2012)

TABLE 5
FITTED PARAMETERS FOR KIC 11395018.

Model	M/M_{\odot}	$(Z/X)_i$	Y_i	α	$t(\text{Gyr})$	L/L_{\odot}	R/R_{\odot}	$T_{\text{eff}}(\text{K})$	$\log g$	[Fe/H]	X_c	χ_{seis}^2	χ_{atm}^2
BA1 (AMP)	1.23	0.034	0.301	1.94	4.46	4.40	2.158	5697	3.860	0.144	0.0	8.07	0.49
BA2 (AMP)	1.32	0.028	0.241	1.94	4.84	4.53	2.210	5671	3.869	0.049	0.0	8.51	0.69
BA3 (AMP) ^a	1.26	0.034	0.294	2.02	4.28	4.64	2.175	5749	3.863	0.140	0.0	7.36	0.55
BB1 (ASTECC1)	1.235	0.033	0.282	1.80	5.05	4.04	2.156	5573	3.861	0.114	0.0	17.03	1.02
BB2 (ASTECC1) ^a	1.22	0.040	0.310	1.80	4.65	4.11	2.154	5605	3.858	0.213	0.0	17.08	1.02
BC1 (ASTECC2)	1.25	0.034	0.297	1.81	4.29	4.42	2.265	5615	3.820	0.116	0.0	47.34	0.90
BC2 (ASTECC2) ^b	1.32	0.043	0.270	1.81	4.89	4.06	2.211	5515	3.870	0.243	0.0	17.65	2.01
BD (CESAM)	1.29	0.030	0.260	0.64 ^c	4.50	4.89	2.190	5806	3.866	0.026	0.0	4.04	1.19
BE (Geneva)	1.32	0.033	0.275	1.80	4.30	5.18	2.207	5867	3.871	0.120	0.0	115.69	1.37
weighted mean	1.27	0.033	0.276		4.57	4.54	2.184	5706	3.863	0.103			
standard dev.	(0.04)	(0.004)	(0.022)		(0.23)	(0.30)	(0.024)	(92)	(0.008)	(0.070)			
Creevey et al. (2012)	1.37±0.11				3.9±1.4 4.5±0.5 ^d	4.2±1.1	2.23±0.04		3.88±0.02 3.86±0.03 ^e				

^a Maximal-list frequencies are used as input.

^b No diffusion is included in this model unlike other ASTEC2 models.

^c Canuto-Goldman-Mazzitelli (CGM) model for turbulent convection (Canuto et al. 1996) is used in this model.

^d This is the value when the average small frequency separation is also used as a seismic constraint.

^e Asteroseismic $\log g$ obtained from scaling relations (Table 7 of Creevey et al. 2012)